Combined Individual Pitch Control and Active Aerodynamic Load Controller Investigation for the 5MW UpWind Turbine

David G. Wilson* Dale E. Berg† Brian R. Resor‡ Matthew F. Barone§ Jonathan C. Berg¶
Sandia National Laboratories P.O. Box 5800, Albuquerque, NM 87185

This paper investigates the combined performance of Individual Blade Pitch (IPC) and Active Aerodynamic Load Control (AALC) applied to the 5MW UpWind reference turbine. IPC is an advanced wind turbine control method for fatigue load reduction. IPC is realized by reducing the 1p blade load through mitigation of the static rotor tilt and yaw moments. AALC uses trailing edge flap devices to reduce fatigue loads or bending moments. This work is motivated by assessing the benefit for the combination of using both approaches one which addresses low frequency (such as the 1p loading) and the other addresses, in addition, higher frequency loading on the blades. This study developed and simulated several IPC and AALC designs to reduce blade loads and potentially pitch duty cycles. The numerical simulations were performed on the NREL 5MW UpWind reference wind turbine model. Two IEC turbulent wind conditions (16 mps and 20 mps) were explored. Results are shown for pitch angles and rates, flap angles and rates, blade flapwise root moments, blade flapwise tip deflections, and flap bending moment power spectral density plots. Other relevant wind turbine components, such as tower moments were also monitored. This study shows that the combined controller designs, when compared with a baseline conventional collective pitch control strategy, demonstrate the trade-offs, load reductions, and potential performance benefits for future large wind turbine control design.

Keywords: Wind turbine control, Trailing edge devices, Independent pitch control, Active aerodynamic load control

I. Introduction

Large turbine sizes will give rise to loads that vary along the blade and change quickly due to wind gusts and other varying wind conditions. Rapidly changing loads can cause fatigue damage and reduce the life of the turbine which in turn may drive the lifetime of all the turbine components. Active pitch control strategies alone, can only control "average" loads on the blade. On the other hand, passive load control strategies cannot respond to local load variations, therefore one must consider active aerodynamic load control as a potential alternative and/or complementary addition to existing strategies. To address these issues, the active aerodynamic load control system design must minimize the error between the desired and actual responses and be capable of providing fast acting control authority over the frequency range of interest.

Previous work that investigates AALC has been performed by the authors and others and can be found in references.[1–4,21] Some of the current investigations and previous work associated with IPC has been performed by Bossanyi[5–7] and others.[8–10] IPC has shown the potential to reduce the 1p loading on large wind turbines. Varying IPC strategies from conventional SISO to modern MIMO designs have been demonstrated. Most recently Lackner and van Kuik[3] have explored and compared IPC and AALC in a side-by-side comparison. Both AALC and IPC were shown to be effective in reducing the fatigue loads on the blades, relative

*Member of Technical Staff, Energy Systems Analysis, dwilso@sandia.gov
†Member of Technical Staff, Wind Energy Technology, deberg@sandia.gov
‡Member of Technical Staff, Wind Energy Technology, brresor@sandia.gov
§Member of Technical Staff, Wind Energy Technology, mbarone@sandia.gov
¶Student Intern, Wind Energy Technology, jcberg@sandia.gov

AWEA WINDPOWER 2009 Conference & Exhibition, Chicago, Illinois, May 4-7, 2009

to the baseline controller. Advantages and disadvantages to both strategies were discussed. However, the main purpose of the research was to address the integration of AALC into wind turbines. The goal of this current research and the subject of this paper is the investigation of advanced independent flap control in combination with exisitng blade pitch control strategies for load reductions. Specifically, how to understand the implications and benefits of active blade control in Region III (above rated power), used to alleviate high frequency dynamics and reduce peak root bending moments. By enabling the trailing edge to move quickly and independently at the outboard portion of the blade then local fluctuations in the aerodynamic forces can be compensated with these trailing edge flaps.

This paper is divided into six sections. Section II provides an overview of the active aerodynamic trailing edge system for blade load control and corrersponding model data. Section III introduces the 5MW UpWind reference wind turbine model used in this study. Section IV discusses the development of the hybrid control system for both IPC and AALC designs. Section V presents the numerical simulation results for the 5MW UpWind turbine utilizing combinations of CPC, IPC, and AALC and Section VI summarizes the results with concluding remarks.

II. Active Aerodynamic Trailing Edge System for Blade Load Control

Active aerodynamic trailing edge devices are one potential solution for blade load reduction. One must consider the sensor distribution along the blade to provide information to the load control devices, distributed along the blade, to respond quickly to alleviate local loads. A control system must be designed to process the sensor information and activate the devices. Initially, for this study, the sensor information is considered to be readily available and the actuator devices are modeled through multiple airfoil tables for lift, drag, and pitch characteristics. In an earlier Sandia study, it was determined that by applying the actuator devices near the blade tip (the outer 25%) would produce the maximum impact. This is shown for the 5.0 MW turbine blade in Fig. 1 which has been modified to include an AALC system to work with the existing collective pitch control system.

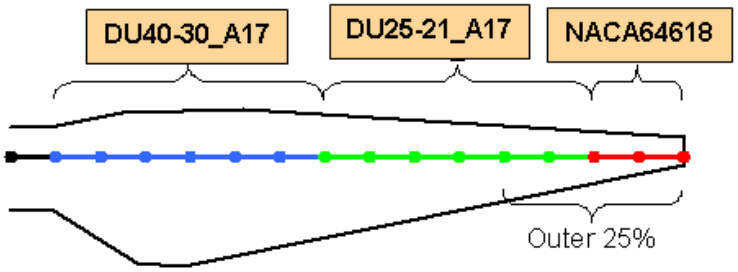

Figure 1. AALC devices located at the outer 25% of span for each blade: 5.0 MW Turbine

The aerodynamic properties of blade sections with active aerodynamic devices required by the FAST code were obtained using the ARC2D code[11] Computational Fluid Dynamics (CFD) code. The ARC2D code, a two-dimensional Navier-Stokes solver, was used to generate aerodynamic lookup tables for lift coefficient, drag coefficient, and pitching moment coefficient for each airfoil geometry of interest, including configurations where the microtab or morphed shape was activated. The CFD results were obtained using the Spalart-Allmaras turbulence model, with specified upper and lower surface boundary layer transition locations. The transition locations were estimated using the XFOIL viscous panel code.[12] The use of CFD allowed for a consistent method for determining changes in airfoil performance with the non-trivial shape changes associated with the active aerodynamic devices. The time required to generate meshes for the CFD calculations of many different shapes was greatly reduced by the use of an automated mesh-generation tool.[13] CFD solutions were obtained over an angle of attack range of -14 degrees to +20 degrees; the airfoil tables were then pre-processed using the AirfoilPrep spreadsheet,[14] which applies the Viterna method to expand the performance tables to the full 360 degree range of angles of attack required by the FAST/Aerodyn codes.

An airfoil with a conventional flap consists of two distinct sections - the fixed leading edge section of the airfoil and a rigid trailing edge section that rotates about the spanwise hinge attached to the leading edge section (see Fig. 2-left). This type of flap has a distinct hinge line, an associated clearance gap (through which air can leak, causing loss of lift and generating noise) and sharp changes or discontinuities in both

the upper and lower surfaces of the airfoil. As a result of these characteristics, the airflow over the airfoil with a deflected flap tends to separate at low angles of attack and create more drag than a morphing trailing edge. FlexSys Inc., of Ann Arbor, Michigan has developed and flight tested a technology that enables them to morph a wing trailing edge.[15,16] That is, they can smoothly and quickly distort the trailing edge of a wing to form an effective flap, while avoiding the discontinuities in the upper and lower wing surfaces, the hinge line and the attendant air gap that are associated with traditional flaps. The morphed flap has a lift characteristic comparable to that of a conventional flap, but with a much reduced drag increment due to flap deflection. Morphing wing cross-section profiles for a 20% chord flap are shown in Fig. 2 (right).

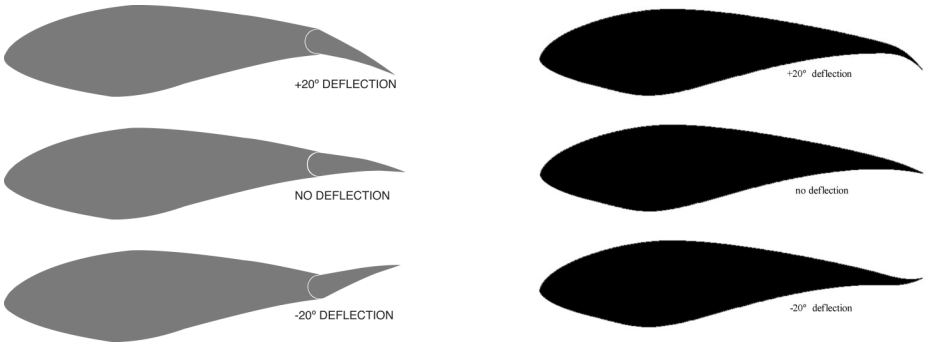

Figure 2. Conventional trailing edge airfoil (left) and morphing wing trailing edge concept (right) with 20% chord ± 20° rotation

III. 5MW UpWind Reference Wind Turbine Model

The 5MW UpWind reference wind turbine characteristics used in this study are given in Table 1 and in reference.[17] The baseline collective pitch control and torque generator control are retained. Both the IPC and AALC were developed as separate control systems and added into the baseline collective pitch control system. The NREL FAST/AeroDyn/Simulink[18] wind turbine dynamics/controls simulation code architecture environment was modified to include the CurveFAST implementation by Larwood[19] and is employed for all control system numerical simulation studies.

Property	Characteristic
Rating	5 MW
Rotor orient, config.	Upwind, 3 Blades
Control	Variable Speed, Collective Pitch
Drivetrain	High Speed, Multi-Stage Gearbox
Rotor, Hub Dia.	126m, 3m
Hub Height	90 m
Cut-In, Rated, Cut-Out Wind Speed	3 m/s, 11.4 m/s, 25 m/s
Cut-In, Rated Rotor Speed	6.9 rpm, 12.1 rpm
Rated Tip Speed	80 m/s
Overhang, Shaft Tilt, Precone	5m, 5°, 2.5°
Rotor Mass	110,000 kg
Nacelle Mass	240,000 kg
Tower Mass	347,460 kg

Table 1 NREL 5MW wind turbine model characteristics

In general terms, the complete nonlinear aero-elastic equations of motion as modeled in FAST/CurveFAST

can be expressed as the following general input-ouput system

$$\begin{aligned} \mathbf{M}(\mathbf{q},\mathbf{u},t)\ddot{\mathbf{q}} + \mathbf{f}(\mathbf{q},\dot{\mathbf{q}},\mathbf{u},\mathbf{u_d},t) &= \mathbf{0} \\ \mathbf{y} &= \mathbf{g}(\mathbf{q},\dot{\mathbf{q}},\mathbf{u},\mathbf{u_d},t) \end{aligned} \tag{1}$$

where $\mathbf{M}$ is the mass matrix, $\mathbf{f}$ is the generalized nonlinear vector state function, $\mathbf{q}$ is the vector of DOF displacements, $\dot{\mathbf{q}}$ is the vector of DOF velocities, $\ddot{\mathbf{q}}$ is the vector of DOF accelerations, $\mathbf{u}$ is the vector of control inputs, $\mathbf{u_d}$ is the vector of disturbance wind inputs, t is time, $\mathbf{g}$ is the generalized nonlinear vector output function, and $\mathbf{y}$ is the measurement vector. The maximum number of variables for the FAST/CurveFAST simulator is extensive and the interested reader is referred to the FAST software and documentation,[18] for complete details. In this development our primary area of interest is in Region III (above rated-power) where IPC is added as a differential pitch angle command to the collective pitch angle command (part of the $\mathbf{u}$ vector). The AALC is considered as a separate independent flap control system based on local feedack information (in this case the tip deflection). The interested reader is referred to reference[1] for more details on how this AALC design was integrated with the current baseline 5MW wind turbine controllers.

IV. Hybrid Pitch/Active Aero Control System Design

In Region III, the baseline Collective Pitch Control (CPC) scheme is used to keep the turbine operating at peak output power while attenuating loads. One of the initial goals of the current project was to minimize the redesign of the control system, yet understand the benefits of introducing both IPC and AALC (with morphing wing trailing edge devices) on the individual blades. Therefore, several combinations of hybrid controllers that include: i) IPC (which uses existing CPC), ii) CPC with AALC (or CPCAA), and iii) IPC with AALC (or IPCAA) are developed and compared with the baseline CPC.

The implementation of IPC uses the d-q transformations defined by Bossanyi.[6] The forward transformation from blade root moments to d-q axis (or tower top yaw and pitch moments) is given as

$$\begin{Bmatrix} M_d \\ M_q \end{Bmatrix} = \frac{2}{3} \begin{bmatrix} \cos(\psi) & \cos(\psi + \frac{2\pi}{3}) & \cos(\psi + \frac{4\pi}{3}) \\ \sin(\psi) & \sin(\psi + \frac{2\pi}{3}) & \sin(\psi + \frac{4\pi}{3}) \end{bmatrix} \begin{Bmatrix} M_{y_1} \\ M_{y_2} \\ M_{y_3} \end{Bmatrix} \tag{2}$$

where ψ is the azimuth angle, $M_{y_i}, (i = 1, 2, 3)$ are the flap root bending moments in the rotating blade coordinate system (as retreived from part of the output vector $\mathbf{y}$), and M_d and M_q are the static yaw and tilt moments in the fixed rotor frame. The signals are then viewed as decoupled and treated as SISO systems for which an integral controller (K_I/s) is designed[9] in series with a notch filter[6] located approximately at the first tower bending modes. The IPC block diagram is shown in Fig. 3.

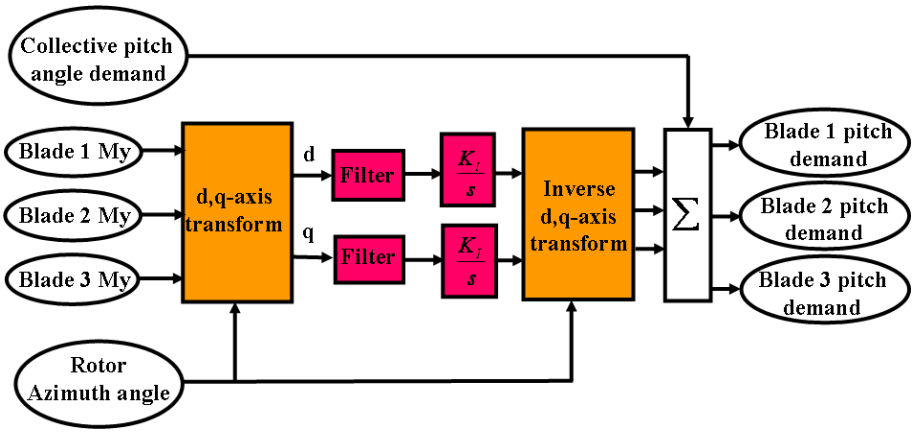

Figure 3. IPC d-q axis transformation implementation with SISO integral controllers and filters

The d-q signals are then inverse transformed by[6]

$$\left\{ \begin{array}{c} \beta_1 \\ \beta_2 \\ \beta_3 \end{array} \right\} = \left[\begin{array}{cc} \cos(\psi) & \sin(\psi) \\ \cos(\psi + \frac{2\pi}{3}) & \sin(\psi + \frac{2\pi}{3}) \\ \cos(\psi + \frac{4\pi}{3}) & \sin(\psi + \frac{4\pi}{3}) \end{array} \right] \left\{ \begin{array}{c} u_d \\ u_q \end{array} \right\} \tag{3}$$

where u_d and u_q are the computed controller signals, and $\beta_i, (i = 1, 2, 3)$ are the individual pitch control signals that are summed with the existing collective pitch control signal and output to the individual blade pitch actuators (through the control vector $\mathbf{u}$). For the IPC design, the controller gains were selected to reduce the 1P loading while observing the same constraints applied to the CPC or

$$0 \leq (\beta_{IPC_i} = \beta_i + \beta_{CPC}) \leq 90^\circ \quad \text{and} \quad \left|\dot{\beta}_{IPC_i}\right| \leq 8^\circ/sec \quad \text{with} \quad i = 1, 2, 3 \tag{4}$$

where β_{CPC} is the baseline collective pitch control command.

The AALC devices all use the same control system structure per each blade which consists of a Proportional-Derivative (PD) feedback design, discussed in.[1] The PD controller uses tip deflection as the feedback signal (from the output vector $\mathbf{y}$). This measurement vector assumes both availability and ideal sensor feedback from the CurveFAST output with no time delay. In addition, a nominal operating point, $y_{tip_{nominal}}$, is included as a reference input signal. The reference input signal is determined by finding the mean value of the tip deflection for the baseline run without AALC. In the future, this signal will be generated based on a running real-time average formulation. Next, an error signal is formulated as $e = (y_{tip} - y_{tip_{nominal}})$ for which the control law becomes

$$\beta_{IFC_i} = -K_{P_i} e_i - K_D \dot{e}_i \tag{5}$$

for $i = 1, 2, 3$. Here β_{IFC} is the commanded flap deflection angle to the trailing edge devices, K_P is the proportional gain, and K_D is the derivative gain. For this work, the active aerodynamic devices are considered fast-acting and capable of responding to high frequency disturbances. Therefore, the augmentation with either the existing low frequency blade CPC or IPC has been seamless, as though decoupled from each other.

In the AALC controller design, the controller gains were selected to optimize maximum power ouput while minimizing blade root flap bending moment oscillations about a mean during turbulent wind conditions. This performance criteria was subject to the requirements to minimize actuator saturation and remain within actuator maximum rate specifications or

$$-10^\circ \leq \beta_{IFC_i} \leq 10^\circ \quad \text{and} \quad \left|\dot{\beta}_{IFC_i}\right| \leq 100^\circ/sec \quad \text{with} \quad i = 1, 2, 3. \tag{6}$$

The actual AALC signal sent to CurveFAST is implemented through the C_D, C_L and C_M aerodynamic load profiles. The aerodynamic loads are applied through the Blade Element Momentum nodes for each blade. In each of the wind turbine cases, the outer 25% of the blade is considered to have AALC capability. Three sets of profiles (pressure-side maximum deployed, neutral, suction-side maximum deployed) are then implemented for this 25% portion of the wind turbine blade. For a calculated controller output value that is between the limits, interpolation is performed within the aerodynamic profiles to determine the corresponding aerodynamic loads to be applied at that instant in time. This interpolation feature is an internal capability within the Aerodyn/CurveFAST interface software. This is considered as a first-order effect implementation. The integration of these AALC devices within the structure and their local deformation responses have not been considered.

The baseline NREL 5MW UpWind FAST model was modified to incorporate AALC and IPC control system and is shown in Fig. 4. Specifically, the first two bending modes are included for the tower fore-aft and side-side DOF's. The first two flap bending modes, the first bending edge mode, and first torsion mode are included for each blade, along with the other baseline DOF's. CurveFAST was used in place of FAST to help monitor the effects of torsion and any coupling that may occur with respect to the trailing edge flap bending actuation. The block in green is the CurveFAST 5MW UpWind plant while all the control system feedback loops are implemented in the Simulink block diagram. The block in orange includes the flap bending moment feedback signals to formulate the IPC implementation as described earlier and shown in Fig. 3.

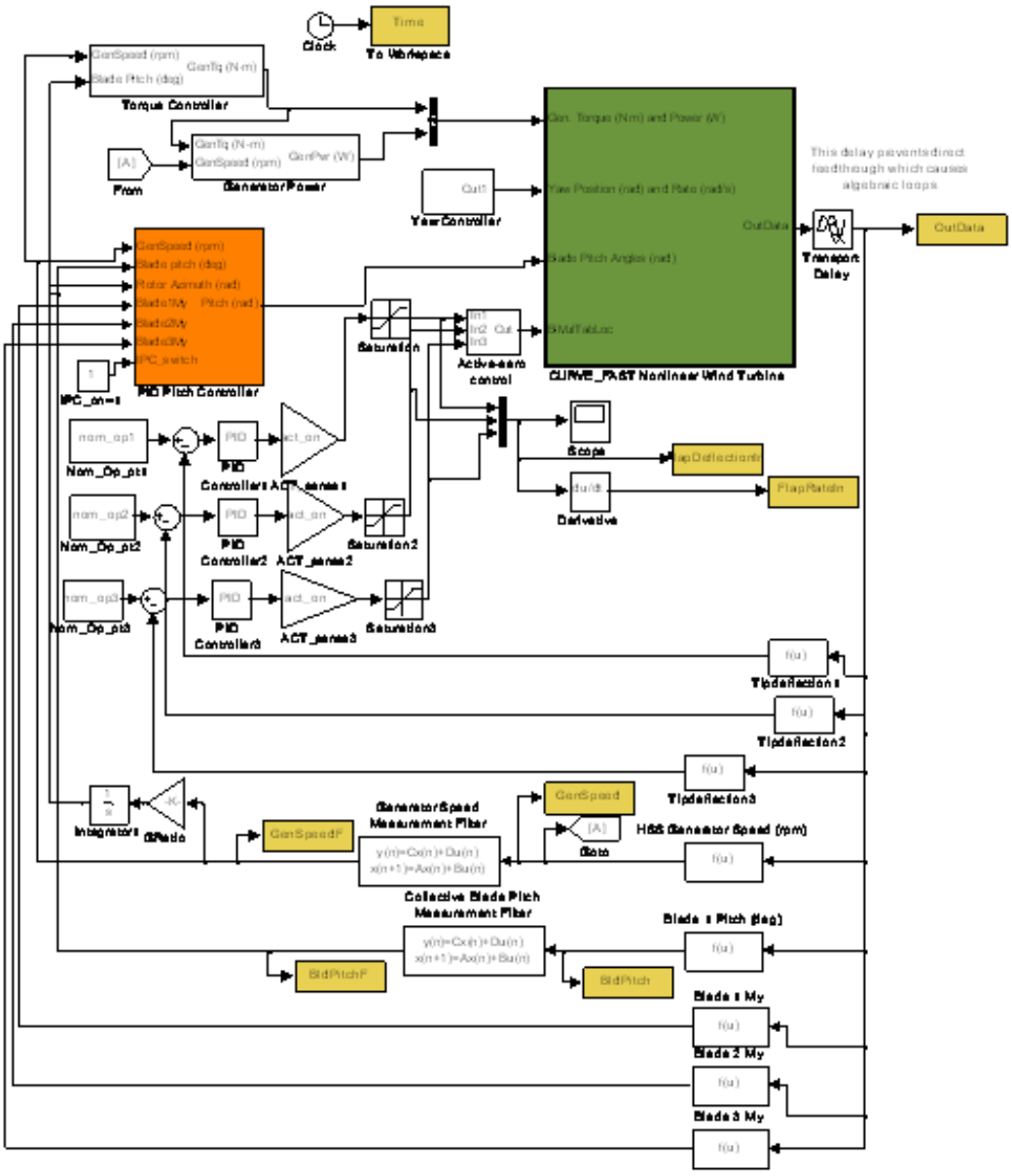

Figure 4. Wind turbine simulator: CurveFAST with augmented IPC and AALC and feedback loops for the 5MW UpWind reference turbine within Matlab/Simulink framework

V. Numerical Simulation Results

The CurveFAST/Simulink modeling environment[18,19] was used to evaluate the hybrid control systems performance for both 16 mps and 20 mps wind conditions in Region III. Figure 5 shows the IEC Normal Turbulence Model (NTM) with Type A (or 16% turbulence intensity) generated with TurbSim[20] (stochastic, full-field, turbulent-wind simulator) used as input to AeroDyn/CurveFAST during all controller evaluations. Ten minute turbulent wind conditions were investigated for all cases (CPC, IPC, CPCAA, and IPCAA). For these discussions a time splice of the final 100 seconds is displayed in all the time domain numerical result responses shown. A summary of the preliminary numerical results for both wind cases are shown for all controller evaluations in Fig. 6. This chart shows the mean wind speed, the standard deviation (STD) for root flap bending moments, with respect to the average value, for each controller. In addition, the percent reduction with respect to CPC is also shown for each controller evaluation (i.e., IPC, CPCAA, and IPCAA). The reduction in root flap bending moment STD's ranged from 14% to 32%. Further data reduction was performed with power spectral density runs and the results are shown for the 16 mps (top) and 20 mps (bottom) cases in Fig. 7. The IPC shows a reduction in the 1p (0.2 Hz) frequency location with respect to

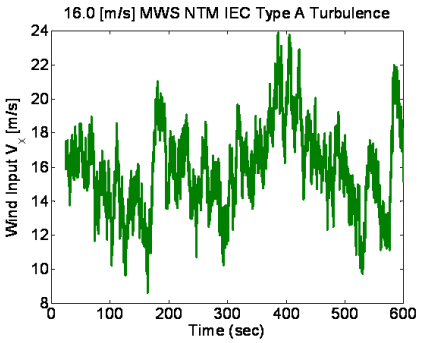

Figure 5. Wind input for 16 mps IEC NTM Type A runs

	CPC	IPC	IPC	CPCAA	CPCAA	IPCAA	IPCAA
Mean Wind Speed	STD kNm	STD kNm	reduced	STD kNm	reduced	STD kNm	reduced
16	2369	2036	-14.0%	1859	-21.54%	1710	-27.81%
20	2727	2182	-19.98%	2136	-21.68%	1849	-32.19%

Figure 6. NTM root flap bending moment reductions preliminary results

the baseline CPC case. The CPCAA case shows a reduction in the 1p frequency with an additional reduction or roll-off in higher frequencies. The IPCAA shows a further reduction beyond both the IPC and CPCAA cases. In the 20 mps case (bottom) the trends are similar with some additonal spread in peaks for the various controller evaluation cases (notably visible at 1p frequency). There has been no attempt to optimize or further partition the frequency bands. With further refinements, it appears possible for the IPCAA case to be able to offload or reduce some of the pitch actuator requirements (from IPC) with the flap actuator system. The small node (see Fig. 7) at about 2 Hz for both the CPCAA and IPCAA (active aero cases) is the second flap bending mode which is still below the earlier resonances.

Next, representative time domain responses are shown for the IPCAA case versus the CPC baseline case. For direct comparisons, the IPCAA cases are shown in blue and the CPC cases are in red. Similar results were also found for the other controller evaluations (IPC and CPCAA with respect to CPC), but are not shown. Figure 8 shows the pitch angle (left) and pitch-rate (right) responses while staying within the specified actuator performance boundaries (as discussed previously). Similar response for the independent flap actuator and actuator rate responses are shown in Fig. 9. Again, these responses fall within the specified performance criteria (also discussed in an earlier section). In Fig. 10 the generator power and rotor speed responses are shown for both cases with minimal variations from the IPCAA controller implementation. Figure 11 shows the blade one root flap moment response (left) and the blade one tip deflection response (right). For the flap moment (left) a reduction of the peak moments of 27.81% can be observed along with a reduction in overall tip deflection (right). Since the combined control systems can potentially couple other degrees-of-freedom associated with the overall wind turbine system, the tower modes (side-to-side and fore-aft) were also checked. Figure 12 shows the tower base side-to-side moment response (left) and the tower base fore-aft moment response (right) with no visible major variations in the time-domain responses. Further data reductions and fatigue load calculations will need to be conducted to help quantify these effects further. Other turbine components such as the LSS torque (left) and the tower top yaw moment (right) were also checked, with the corresponding responses shown in Fig. 13.

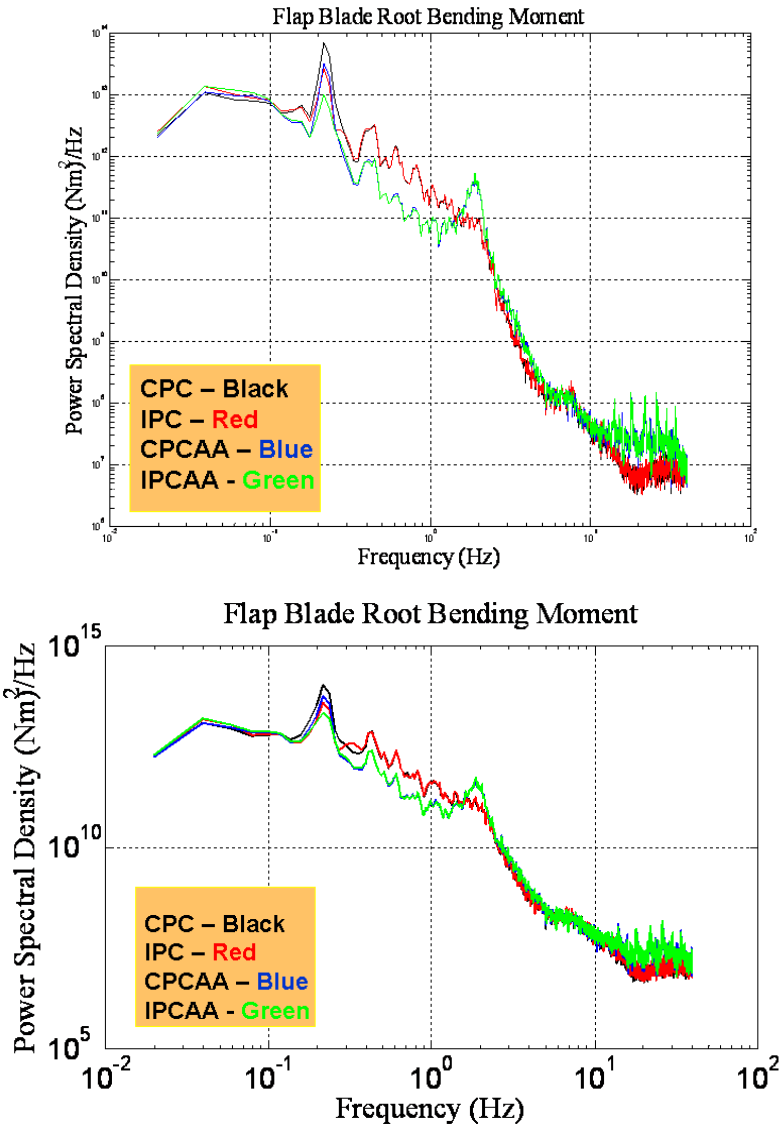

Figure 7. PSD preliminary results: all cases 16 mps (top) and 20 mps (bottom) wind conditions

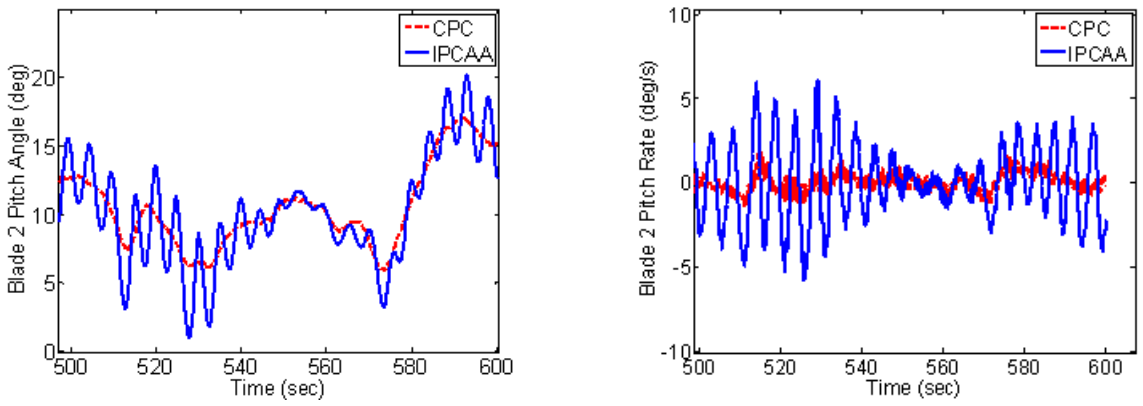

Figure 8. Numerical simulation results 16 mps case: blade 2 pitch angle response (left) and pitch-rate response (right)

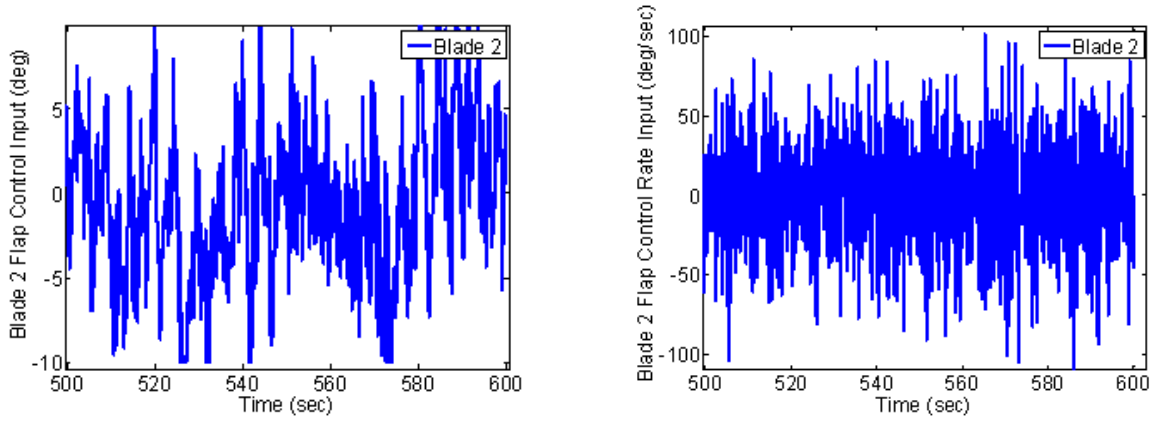

Figure 9. Numerical simulation results 16 mps case: blade 2 flap angle response (left) and flap-rate response (right)

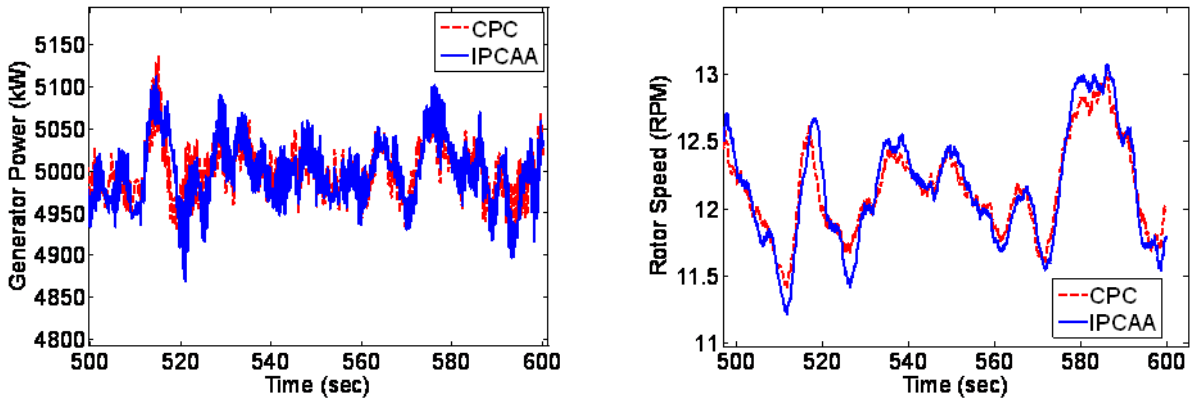

Figure 10. Numerical simulation results 16 mps case: generator power response (left) and rotor speed response (right)

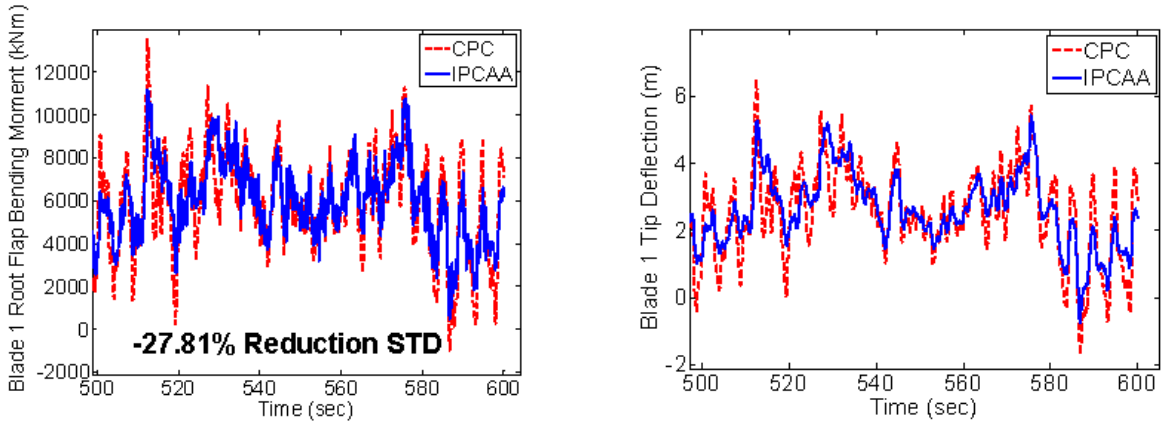

Figure 11. Numerical simulation results 16 mps case: blade 1 root flap moment response (left) and blade 1 tip deflection response (right)

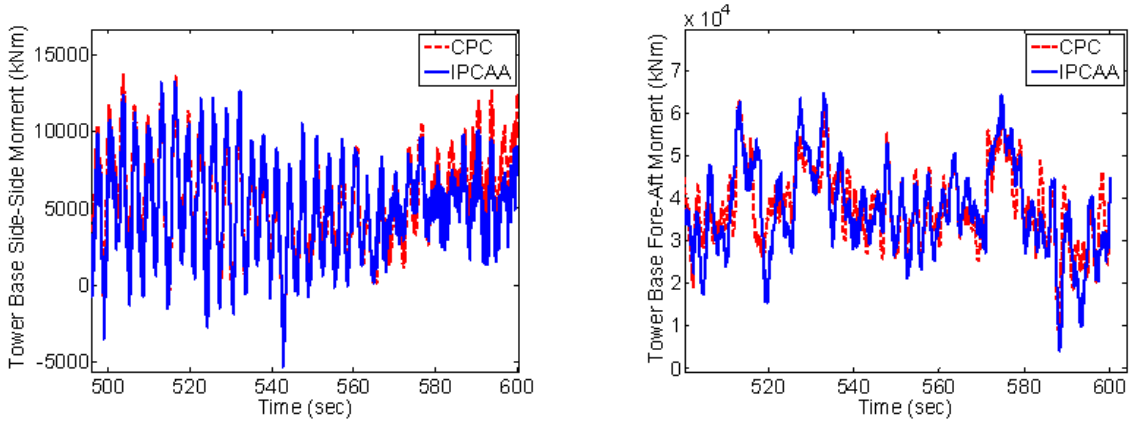

Figure 12. Numerical simulation results 16 mps case: tower base side-to-side moment response (left) and tower base fore-aft moment response (right)

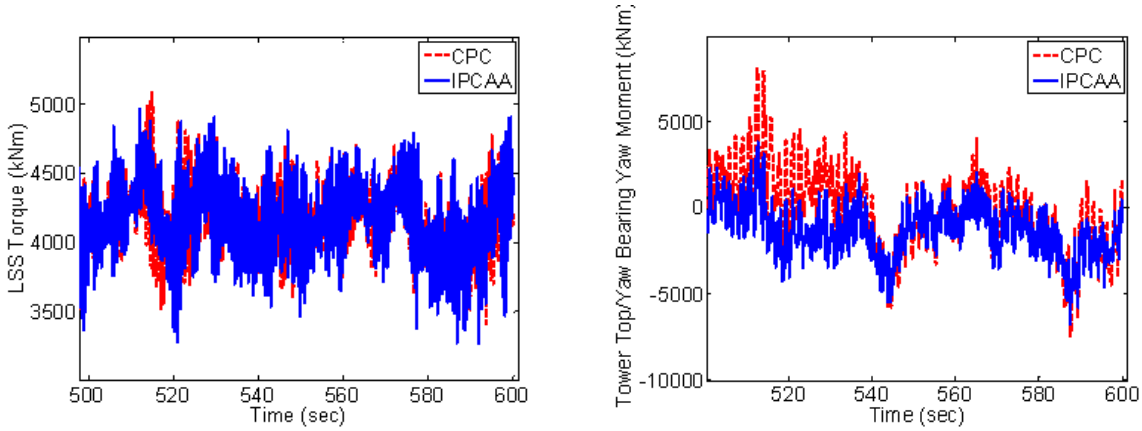

Figure 13. Numerical simulation results 16 mps case: LSS torque response (left) and yaw moment response (right)

As a direct result of the d-q transformation to the fixed rotor reference frame, the static tilt (left) and yaw (right) moments are available and are shown in Fig. 14. The goal of the IPC controller is to regulate these moments about zero. From these responses the IPCAA has visibly pulled the average down closer to the reference zero line, along with reducing the peaks. As a final check the torsional twist at the tip of blade

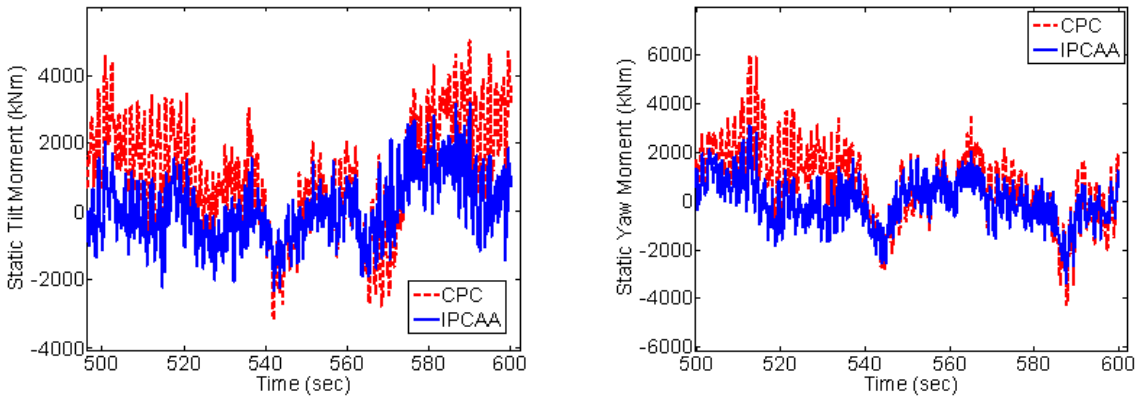

Figure 14. Numerical simulation results 16 mps case: static tilt moment response (left) and static yaw moment response (right)

is available as output from CurveFAST and is shown in Fig. 15. This response shows minimal variations from the baseline, indicating that the torsion mode is not currently affected by the operation of the AALC.

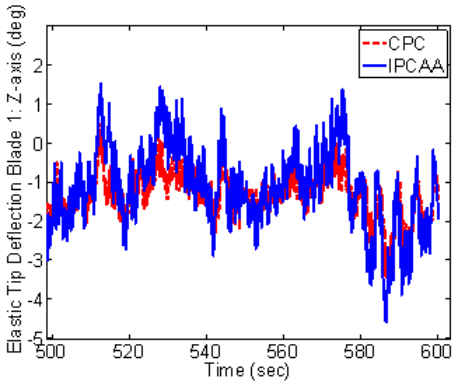

Figure 15. Numerical simulation result 16 mps case: elastic tip deflection response

VI. Summary and Conclusions

This paper has shown the feasibility for employing active aerodynamic devices for load alleviation in combination with other collective and/or independent pitch control systems. This included the morphing wing trailing edge devices with 20% chord that were incorporated into the 5MW NREL UpWind reference turbine. CurveFAST was used for all the numerical simulation runs and helped to verify that no adverse affects resulted due to the torsional blade DOF. A general trend for all the controller evaluations was that the root flap bending moments, were reduced, ranging from 14-32%, in STD oscillations from the mean value. This included the independent pitch control, collective pitch control with active aerodynamic load control, and independent pitch control with active aerodynamic load control. In addition, other critical wind turbine components, such as the tower moments, LSS torque, tower-top yaw moment, etc., were not adversely affected with the various controller design evaluations. In particular, it was demonstrated that by using active aerodynamic devices, substantial benefits for future wind turbine designs can be realized. Future work will include further investigations of fatigue loading compilation and calculations and evaluation of other promising active aerodynamic trailing edge designs.

Acknowledgments

The authors would like to thank Dr. Scott Larwood of Purlwind Consulting for the development and use of CurveFAST, Professor Case van Dam, UC Davis and Mr. Jose Zayas, Manager, Wind Energy Technology Dept., Sandia National Labs, for earlier discussions on active aero devices, and Professor Sridhar Kota at FlexSys, Inc., for their development and use of the morphing wing trailing edge work. Sandia National Laboratories is a multiprogram laboratory operated by Sandia Corporation, a Lockheed Martin Company, for the U.S. Department of Energy's National Nuclear Security Administration under contract DE-AC04-94AL85000.

References

[1]D.G. Wilson, D.E. Berg, M.F. Barone, J.C. Berg, B.R. Resor, and D.W. Lobitz, *Active Aerodynamic Blade Control Design for Load Reduction on Large Wind Turbines*, European Wind Energy Conference & Exhibition, Marseille, France, March 2009.

[2]D.E. Berg, D.G. Wilson, J.C. Berg, B.R. Resor, M.F. Barone, J.R. Zayas, S. Kota, G. Ervin, and D. Maric, *The Impact of Active Aerodynamic Load Control on Wind Energy Capture at Low Wind Speed Sites,* European Wind Energy Conference & Exhibition, Marseille, France, March 2009.

[3]M.A. Lackner and G. van Kuik, *A Comparison of Smart Rotor Control Approaches using Trailing Edge Flaps and Individual Pitch Control*, 47th AIAA Aerospace Sciences Meeting, Jan 2009, Orlando, Florida.

[4]T.K. Barlas and G. van Kuik, *Aeroelastic Modeling and Comparison of Advanced Active Flap Control Concepts for Load Reduction on the Upwind 5MW Wind Turbine*, European Wind Energy Conference & Exhibition, Marseille, France, March 2009.

[5]E. Bossanyi and D. Witcher, *A state-of-the-art Controller for the 5MW UpWind Reference Wind Turbine*, European Wind Energy Conference & Exhibition, Marseille, France, March 2009.

[6]E. Bossanyi, *Individual Blade Pitch Control for Load Reduction*, Wind Energy, 2003, 6:119-128.

[7]E. Bossanyi, *Further Load Reductions with Individual Pitch Control*, Wind Energy, 2005, 8:481-485.

[8]K. Selvam, *Individual Pitch Control for Large Scale Wind Turbines: Multivariable Control Approach*, ECN-E-07-053.

[9]T.G. van Engelen *Design Model and Load Reduction Assessment for Multi-Rotational Mode Individual Pitch Control (Higher Harmonics Control)*, European Wind Energy Conference & Exhibition, Athens, Greece, March 2006.

[10]M. Geyler and P. Caselitz, *Robust Multivariable Pitch Control Design for Load Reduction on Large Wind Turbines*, ASME Journal of Solar Energy Engineering, Aug. 2008, Vol. 130.

[11]T.H. Pulliam, *Efficient Solution Methods for the Navier-Stokes Equations*, Lecture Notes for the von Karman Institute for Fluid Dynamics Lecture Series: Numerical Techniques for Viscous Flow Computation in Turbomachinery Bladings, von Karman Institute, Rhode-St-Genese, Belgium., 1986.

[12]M. Drela and M.B. Giles, *Viscous-Inviscid Analysis of Transonic and Low Reynolds Number Airfoils*, AIAA J, 25(10):1347-1355, 1987.

[13]S.Y. Yoo, *Integrated Method of CFD and Grid Generation for Automatic Generation of Airfoil Performance Tables*, M.S. Thesis, Mechanical and Aeronautical Engineering Department, University of California-Davis, 2008.

[14]NWTC Design Codes (AirfoilPrep by Dr. Craig Hansen). http://wind.nrel.gov/designcodes/preprocessors/airfoilprep/. Last modified 16-January-2007; accessed 16-January-2007.

[15]S. Kota, J.A. Hetrick, R. Osborn, D. Paul, E. Pendleton, P. Flick, and C. Tilmann, *Design and Application of Compliant Mechanisms for Morphing Aircraft Structures*, Smart Structures and Materials 2003: Industrial and Commercial Applications of Smart Structures Technologies, Eric H. Anderson, Editor, Proceedings of SPIE Vol. 5054, 2003.

[16]J.A. Hetrick, R.F. Osborn, S. Kota, P.M. Flick, D.B. Paul, *Flight Testing of Mission Adaptive Compliant Wing*, 48th AIAA/ASME/ASCE/AHS/ASC Structures, Structural, April 2007, Honolulu, Hawaii, AIAA 2007-1709.

[17]J.M. Jonkman, S. Butterfield, W. Musial, and G. Scott, *Definition of a 5-MW Reference Wind Turbine for Offshore System Development*, Technical Report, NREL/TP-500-38060, Feb. 2009.

[18]J.M. Jonkman and M.L. Buhl, Jr., *FAST User's Guide*, NREL Technical Report, NREL/EL-500-38230, August 2005.

[19]S.M. Larwood, *Dynamic Analysis Tool Development for Advanced Geometry Wind Turbine Blades*, PhD Disseration, Mechancial and Aeronatuical Engineering, University of California, Davis, 2009.

[20]B.J. Jonkman and M.L. Buhl, Jr., *TurbSim User's Guide for version 1.40*, Technical Report NREL/TP-xxx, Sept. 2008.

[21]T. Buhl, M. Gaunaa, and P.B. Andersen, *Stability Limits for a Full Wind Turbine Equipped with Trailing Edge Systems*, European Wind Energy Conference & Exhibition, Marseille, France, March 2009.